Scholars Journal of Physics, Mathematics and Statistics

OPEN ACCESS

Abbreviated Key Title: Sch J Phys Math Stat
ISSN 2393-8056 (Print) | ISSN 2393-8064 (Online)
Journal homepage: https://saspublishers.com

Anisotropic Cosmological Model in Brans-Dicke Theory of Gravitation

M.R. Ugale[1], H.A. Nimkar[1*], A.O. Dhore[2]

[1]Department of Science and Humanities, Sipna College of Engineering & Technology, Amravati, 444701, Maharashtra, India
[1]Department of Applied Science and Humanities, Dr. Rajendra Gode Institute of Technology & Research, Amravati, 444602, Maharashtra, India
[2]Department of Mathematics, Shri. Dr. R.G. Rathod Arts and Science College, Murtizapur, Dist. Akola, 444107, Maharashtra, India

DOI: https://doi.org/10.36347/sjpms.2025.v12i08.003 | **Received:** 08.07.2025 | **Accepted:** 01.09.2025 | **Published:** 15.09.2025

***Corresponding author:** H.A. Nimkar
Department of Science and Humanities, Sipna College of Engineering & Technology, Amravati, 444701, Maharashtra, India

Abstract | **Review Article**

In this paper, we study an anisotropic cosmological model in scalar tensor theory of gravitation proposed by Brans-Dicke, considering a Bianchi type-II spacetime geometry filled with a macroscopic body. To solve the nonlinear Brans-Dicke field equations by using the average scale factor and the relation between metric coefficients, with a radiation universe, we obtained exact solutions for the metric functions and scalar field. We derive and analyze several key cosmological parameters as functions of redshift, including the Hubble parameter, expansion scalar, shear scalar, energy density, pressure and the Brans-Dicke scalar field. The evolution of these parameters is graphically illustrated, revealing that the model predicts an expanding universe with dynamics transitioning from an early decelerating phase to a late-time acceleration. The behavior of the deceleration parameter supports the accelerated expansion in accordance with current observational data. Furthermore, we investigate higher-order cosmological diagnostics such as the jerk and snap parameters as well as the statefinder parameters (r,s), which are instrumental in distinguishing this model from the standard ΛCDM cosmology and other dark energy models. We also explore the Om diagnostic to characterize dark energy evolution and compare our theoretical Hubble parameter values with a compilation of 57 recent Hubble dataset points obtained from differential age *(DA)* and baryonic acoustic oscillation *(BAO)* methods. A good agreement is observed between the model predictions and observational data, as indicated by the best-fit curve with minimal root mean square error.

Keywords: Bianchi type-II, Brans-Dicke Theory, Macroscopic Body, Cosmological Parameter.

1. INTRODUCTION

The Brans-Dicke theory [1] is the most natural choice as the scalar-tensor theory, which can be considered as a pioneer in the study of scalar-tensor theories, the inclusion of Mach's principal led to the advent of this theory. This can be called the first-ever theory of gravity, where the metric tensor represents the dynamics of spacetime and the scalar field describes the dynamics of gravity. The Brans-Dicke theory describes the recent accelerated expansion of the universe and accommodates the observational data. In this theory, the scalar field ϕ is time-dependent, it is analogous to $8\pi G^{-1}$. Therefore, in Brans-Dicke scalar-tensor theory, the scalar field ϕ couples to the gravity with a dimensionless coupling parameter ω. Many authors have discussed several aspects of Brance-Dicke theory viz., Sharma *et al.,,* [2], Ahmadi-Azar *et al.,,* [3], Mishra *et al.,,* [4], Santhi *et al.,,* [5], Satyanarayana *et al.,,* [6], Gaidhane *et al.,,* [7], Bamba *et al.,,* [8], Nimkar *et al.,,* [9], Halife caglar [10], Vijayasanthi *et al.,,* [11-12], Kapse *et al.,,* [13], Bhardwaj *et al.,,* [14], Trivedi *et al.,,* [15], singh *et al.,,* [16 -18], Saha *et al.,,* [19], Shaikh *et al.,,* [20], Rani *et al.,,* [21], Pawar *et al.,,* [22], Tirandari *et al.,,* [23], Rao *et al.,,* [24], Chirde *et al.,,*[25-26], Pawar *et al.,,* [27-28], Reddy *et al.,,* [29-30], Wankhade *et al.,,* [31], Vidyasagar *et al.,,* [32-33], Ghate *et al.,,* [34], Adhav *et al.,,* [35-36].

Brans- Dicke field equations for combined scalar and tensor fields are

$$G_{ij} = -8\pi\phi^{-1}T_{ij} - \omega\phi^{-2}\left(\phi_{,i}\phi_{,j} - \frac{1}{2}g_{ij}\phi_{,k}\phi^{,k}\right) - \phi^{-1}\left(\phi_{i;j} - g_{ij}\phi^{,k}_{;k}\right) \quad (1)$$

And

$$\phi = \phi^{,k}_{;k} = \frac{8\pi\phi^{-1}T}{(3+2\omega)} \quad (2)$$

Where $G_{ij} = R_{ij} - \frac{1}{2}g_{ij}R$ is an Einstein tensor, T_{ij} is the stress-energy tensor of the matter, ω is the dimensionless coupling constant, comma and semi-colon denote partial and covariant differentiation respectively. In addition, we have energy conservation equation.

$$T^{ij}_{;j} = 0 \quad (3)$$

This equation is a consequence of the field equations (1) and (2).

Bianchi-type model have been studied by several authors in an attempt to understand anisotropy in the universe. The same models have also been used to examine the role of certain anisotropic sources during the formation of the large-scale structure in the universe today. Tinker [37], Chirde *et al.,* [38], Bhoyar *et al.,* [39], Sharma *et al.,* [40], Singh *et al.,* [41-42], Pradhan *et al.,* [43], Agarwal *et al.,* [44], Singh *et al.,* [45], Banerjee *et al.,* [46] are some of the authors who studied Bianchi type II cosmological model. Also, Wath *et al.,* [47], have obtained stability of macroscopic body cosmological model in Ruban's background. Nimkar *et al.,* [48], have Studied Stability of cosmological model in self- creation theory of gravitation. Hadole *et al.,* [49], has examined the microscopic body cosmological model.

The current work aims to get a Bianchi type- II cosmological model with Brans-Dicke theory of gravitation in the presence of a macroscopic body. The present paper is organized as follows. In section 2, Metric and field equations. Section 3, Solutions of field equations, Section 4, is mainly concerned with the physical and kinematical properties of the model, and the last section contains conclusions.

2. Metric and Field Equations

Consider the metric for Bianchi type-II Space-time in the general form

$$ds^2 = dt^2 - A^2(dx - zdy)^2 - B^2dy^2 - C^2dz^2 \quad (4)$$

Where the metric potentials A, B and C are functions of cosmological time t.

The energy-momentum tensor for a macroscopic body (Landau L.D. and Lifshitz E.M.) [50] is given by

$$T^{ik} = (p+\varepsilon)u^iu^k - pg^{ik} \quad (5)$$

Here p is the pressure, ε is the energy density and u_i is the four-velocity vector of the distribution, respectively. From eq. (5) we have

$$T^1_1 = T^2_2 = T^3_3 = -p,\ T^4_4 = \varepsilon\,. \quad (6)$$

The trace of the energy-momentum tensor is given by

$$T^1_1 + T^2_2 + T^3_3 + T^4_4 = -3p + \varepsilon \quad (7)$$

Using the eq. (1), (2) and (5)-(7), the field equations for metric (4) are

$$\frac{\ddot{B}}{B} + \frac{\ddot{C}}{C} + \frac{\dot{B}\dot{C}}{BC} - \frac{3A^2}{4B^2C^2} + \frac{\omega}{2}\left(\frac{\phi_4}{\phi}\right)^2 + \left(\frac{\dot{B}}{B} + \frac{\dot{C}}{C}\right)\frac{\phi_4}{\phi} + \frac{\phi_{44}}{\phi} = -8\pi\phi^{-1}p \quad (8)$$

$$\frac{\ddot{A}}{A} + \frac{\ddot{C}}{C} + \frac{\dot{A}\dot{C}}{AC} + \frac{A^2}{4B^2C^2} + \frac{\omega}{2}\left(\frac{\phi_4}{\phi}\right)^2 + \left(\frac{\dot{A}}{A} + \frac{\dot{C}}{C}\right)\frac{\phi_4}{\phi} + \frac{\phi_{44}}{\phi} = -8\pi\phi^{-1}p \quad (9)$$

$$\frac{\ddot{A}}{A} + \frac{\ddot{B}}{B} + \frac{\dot{A}\dot{B}}{AB} + \frac{A^2}{4B^2C^2} + \frac{\omega}{2}\left(\frac{\phi_4}{\phi}\right)^2 + \left(\frac{\dot{A}}{A} + \frac{\dot{B}}{B}\right)\frac{\phi_4}{\phi} + \frac{\phi_{44}}{\phi} = -8\pi\phi^{-1}p \quad (10)$$

$$\frac{\dot{A}\dot{B}}{AB} + \frac{\dot{B}\dot{C}}{BC} + \frac{\dot{A}\dot{C}}{AC} - \frac{A^2}{4B^2C^2} - \frac{\omega}{2}\left(\frac{\phi_4}{\phi}\right)^2 + \left(\frac{\dot{A}}{A} + \frac{\dot{B}}{B} + \frac{\dot{C}}{C}\right)\frac{\phi_4}{\phi} = 8\pi\phi^{-1}\varepsilon \quad (11)$$

By solving eq. (2) we get,

$$\phi_{44}+\phi_4\left(\frac{\dot{A}}{A}+\frac{\dot{B}}{B}+\frac{\dot{C}}{C}\right)=\frac{8\pi}{\phi}\frac{(\varepsilon-3p)}{(3+2\omega)} \qquad (12)$$

and the eq. (3) takes the form

$$\dot{\varepsilon}+(\varepsilon+p)\left(\frac{\dot{A}}{A}+\frac{\dot{B}}{B}+\frac{\dot{C}}{C}\right)=0 \qquad (13)$$

Where, the upper suffix dot denotes differentiation with respect to t .

3. Solutions of Field Equations

The above four independent eq. (8) to (11) are highly nonlinear consist of six unknowns A,B,C,ϕ,p and ε . To get a determinate solution, we require two conditions; the relation between metric coefficients, i.e., $B=A^m$ and $C=A^n$ where m and n are arbitrary constant and the equation of state by Singh [41].

The average scale factor $a(t)$ and proper volume V for Bianchi Type II Space-time are as follows:

$$a(t)=(ABC)^{\frac{1}{3}}=(A)^{\frac{m+n+1}{3}} \qquad (14)$$

$$V=[a(t)]^3=ABC=(A)^{\frac{m+n+1}{3}} \qquad (15)$$

Directional Hubble parameters

$$H_x=\frac{\dot{A}}{A},H_y=\frac{\dot{B}}{B},H_z=\frac{\dot{C}}{C} \qquad (16)$$

Average Hubble Parameter $H=\frac{\dot{a}}{a}$ (17)

Scalar expansion $\theta=3H$ (18)

Shear Scalar $\sigma^2=\frac{1}{2}\sigma^{ij}\sigma_{ij}$ (19)

Now, consider a generalized linearly varying deceleration parameter (Akarsu and Dereli)[51]. This is as follows;

$$q=-\frac{a\ddot{a}}{\dot{a}^2}=-rt+\alpha-1 \qquad (20)$$

Where $r\geq 0$ and $\alpha\geq 0$ are constant and $r=0$ reduces to the law of Berman [52], which yields models with constant deceleration parameters.

$a(t)=k_2(\gamma t+k_1)^{\frac{1}{\alpha}}$, for $r=0$ and $\alpha>0$ (21)

From eq. (14) and (21) we get

$$A=k_2^{\frac{3}{(m+n+1)}}(\gamma t+k_1)^{\frac{3}{\alpha(m+n+1)}} \qquad (22)$$

$$B=k_2^{\frac{3m}{(m+n+1)}}(\gamma t+k_1)^{\frac{3m}{\alpha(m+n+1)}} \qquad (23)$$

$$C=k_2^{\frac{3n}{(m+n+1)}}(\gamma t+k_1)^{\frac{3n}{\alpha(m+n+1)}} \qquad (24)$$

Bianchi type II metric for this model takes the form,

$$ds^2=dt^2-\left[k_2^{\frac{3}{(m+n+1)}}(\gamma t+k_1)^{\frac{3}{\alpha(m+n+1)}}\right]^2(dx-zdy)^2-\left[k_2^{\frac{3m}{(m+n+1)}}(\gamma t+k_1)^{\frac{3m}{\alpha(m+n+1)}}\right]^2dy^2-\left[k_2^{\frac{3n}{(m+n+1)}}(\gamma t+k_1)^{\frac{3n}{\alpha(m+n+1)}}\right]^2dz^2 \qquad (25)$$

4. The Physical and Kinematical Properties of the Model

Redshift is a highly significant and often contentious phenomenon regarding cosmology and astronomy. When electromagnetic radiation from an object is directed towards the less energetic regions of the spectrum, a phenomenon known as the shift in electromagnetic radiation occurs. We utilized this phenomenon to get insight into aspects of our galaxy and even the whole universe. The relation between average scale factor a with redshift z are connected through the relation is

$$1+z=\frac{a_0(t)}{a(t)} \tag{26}$$

Where $a_0(t)$ is the present value of the scale factor, take $a_0(t)=1.$ using eq. (21) and the relation $a(t)=\frac{1}{1+z}$ with z being the redshift gives us the following relation:

$$t=\frac{1}{\gamma}\left[\left(\frac{k_2}{1+z}\right)^{\alpha}-k_1\right] \tag{27}$$

In this section, we have estimated and determined significant cosmological quantities in connection to redshift. These computations aid our understanding of the expansion of the universe, energy distribution, and the effects of many components at various redshifts.

The key cosmological parameters, Hubble parameter (H), expansion scalar (θ), shear scalar (σ^2) in terms of redshift are calculated as

$$H=\frac{\gamma(1+z)^{\alpha}}{\alpha k_2^{\alpha}} \tag{28}$$

$$\theta=\frac{3\gamma(1+z)^{\alpha}}{\alpha k_2^{\alpha}} \tag{29}$$

$$\sigma^2=\frac{3\gamma^2(1+z)^{2\alpha}}{2\alpha^2 k_2^{2\alpha}} \tag{30}$$

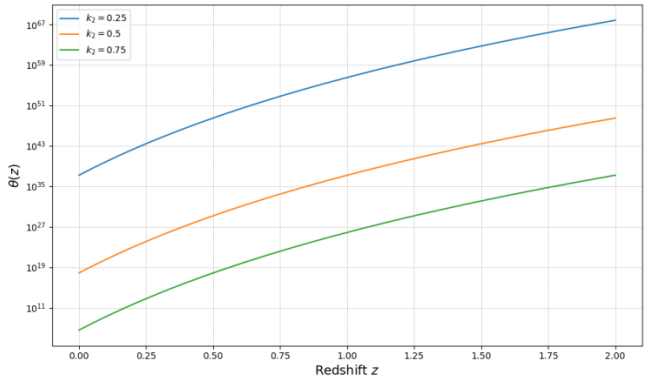

Fig.1 Expansion Scalar Vs. redshift

$k_2 = 0.5, \gamma = 0.743, \alpha = 64.152$

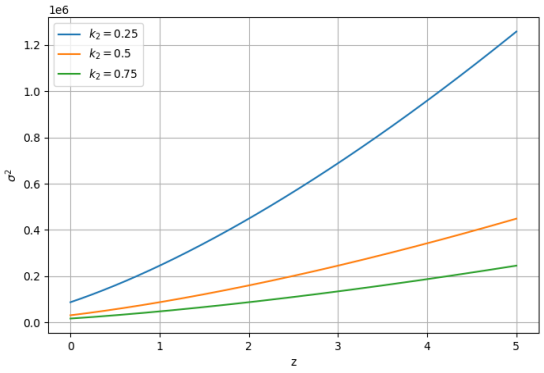

Fig.2 Shear Scalar Vs. redshift

$k_2 = 0.5, \gamma = 0.743, \alpha = 64.152$

From Fig.1 it is observed that the scalar expansion $\theta(z)$ grows rapidly as we go back in time (higher redshift), indicating a faster-expanding early universe. Lower values of the parameter k_2 correspond to significantly higher expansion rates, suggesting that k_2 controls the intensity of expansion. As k_2 increases, the expansion is more moderated. This behavior supports a dynamic expansion history, potentially linked to dark energy or modified gravity effects influencing the cosmic evolution. Fig. 2 The graph shows the variation of shear scalar σ^2 with redshift z for different values of k_2 as z increases, σ^2 increases, indicating that the universe was more anisotropic in the past. At present (z = 0), σ^2 is minimal, suggesting a nearly isotropic

universe today. Lower values of k_2 result in higher σ^2 meaning stronger anisotropic effects in the early universe. As k_2 increases, anisotropy decreases. This reflects that the universe has evolved from a highly anisotropic phase to a more isotropic one over time.

Also, the Scalar field is as follows

$$\phi = k_3\left(\frac{k_2}{1+z}\right)^{(\alpha-3)} \quad \text{Where, } k_3 = \frac{k}{k_2^3\left(\frac{\alpha-3}{\alpha}\right)\gamma} \tag{31}$$

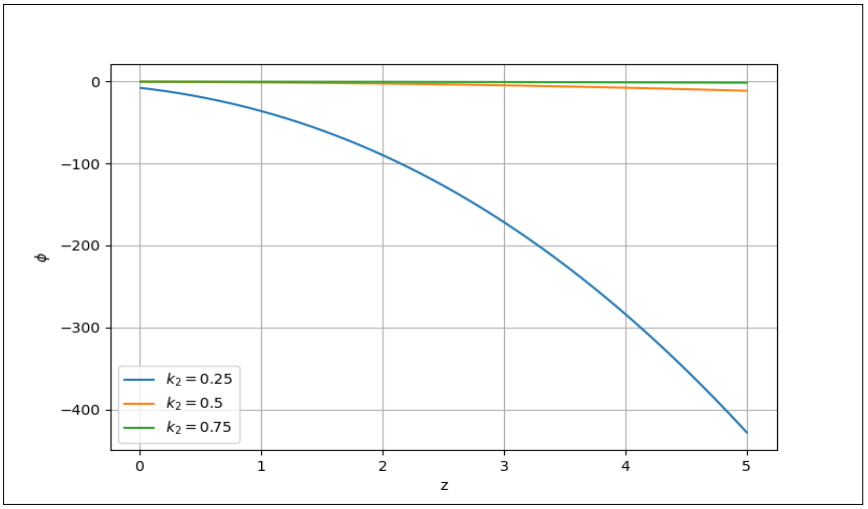

Fig. 3: Scalar field Vs. redshift $k_2 = 0.5, k_3 = 1, \alpha = 64.152$

From fig (3), it is observed initially k_2 at low redshift (near present), ϕ is close to zero for all k_2 values, indicating a stable universe. As redshift increases, ϕ becomes more negative, especially for lower k_2, showing stronger dynamical evolution in the early universe. For $k_2 = 0.25$, the drop is steep, suggesting a rapidly changing cosmic behavior in the past. For higher k_2 the change is minimal, pointing to a more stable early state. The graph implies that the value of k_2 significantly affects the universe's expansion history. Pressure and energy density are given by

$$p = -\frac{k_3 k_2^{(\alpha-3)}}{8\pi(1+z)^{\alpha-3}}\left\{\begin{array}{l}\left(\frac{\psi_1(1+z)^{\frac{6}{(m+n+1)}}}{k_2^{\frac{12}{(m+n+1)}}} - \frac{3(1+z)^{\frac{6(m+n-1)}{(m+n+1)}}}{4\left(k_2^{\frac{12(m+n-1)}{(m+n+1)}}\right)} + \frac{\omega}{2}\left[\frac{(\alpha-3)^2\gamma^2(1+z)^{2\alpha}}{\alpha^2 k_2^{2\alpha}}\right]\right) + \\ \left[\frac{(m+n)(1+z)^{\frac{3}{(m+n+1)}}}{k_2^{\frac{6}{(m+n+1)}}}\right]\frac{(\alpha-3)\gamma(1+z)^{\alpha}}{\alpha k_2^{\alpha}} - \frac{3(\alpha-3)(1+z)^{2\alpha}\gamma^2}{\alpha^2 k_2^{2\alpha}}\end{array}\right\} \tag{32}$$

$$\varepsilon = -\frac{3k_3 k_2^{(\alpha-3)}}{8\pi(1+z)^{\alpha-3}}\left\{\begin{array}{l}\left(\frac{\psi_1(1+z)^{\frac{6}{(m+n+1)}}}{k_2^{\frac{12}{(m+n+1)}}} - \frac{3(1+z)^{\frac{6(m+n-1)}{(m+n+1)}}}{4\left(k_2^{\frac{12(m+n-1)}{(m+n+1)}}\right)} + \frac{\omega}{2}\left[\frac{(\alpha-3)^2\gamma^2(1+z)^{2\alpha}}{\alpha^2 k_2^{2\alpha}}\right]\right) + \\ \left[\frac{(m+n)(1+z)^{\frac{3}{(m+n+1)}}}{k_2^{\frac{6}{(m+n+1)}}}\right]\frac{(\alpha-3)\gamma(1+z)^{\alpha}}{\alpha k_2^{\alpha}} - \frac{3(\alpha-3)(1+z)^{2\alpha}\gamma^2}{\alpha^2 k_2^{2\alpha}}\end{array}\right\} \tag{33}$$

Where, $\psi_1 = m(m-1)+n(n-1)+mn$

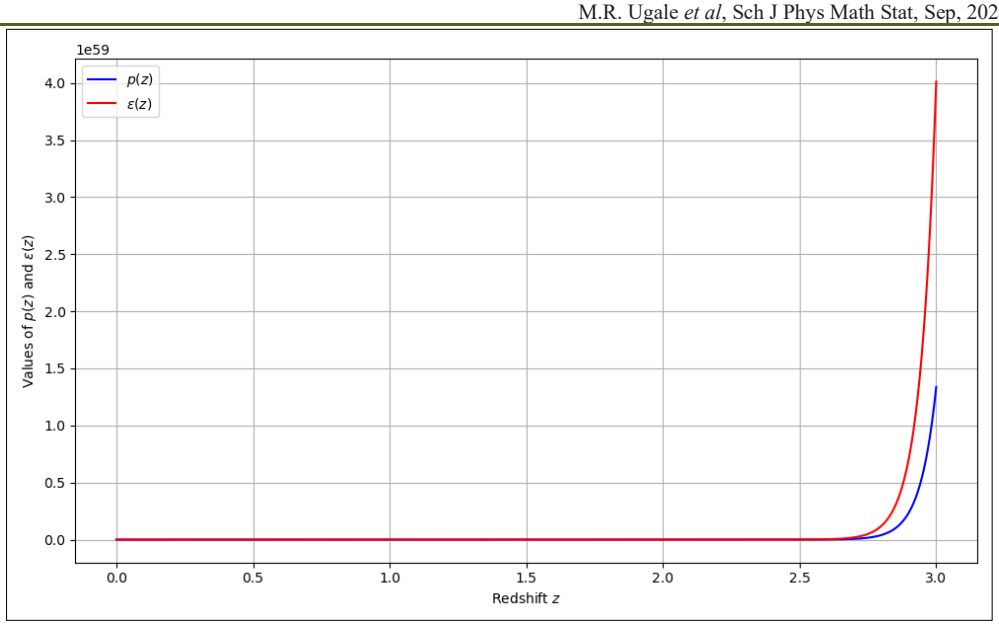

Fig 4. Pressure p and Energy Density ε vs redshift z .

$k_2 = 0.5, k_3 = 1, \gamma = 0.743, \alpha = 64.152, \omega = 0.1, , m = n = 1$

From fig. (4) We can observe that both pressure $p(z)$ and energy density $\varepsilon(z)$ increase sharply with redshift z especially beyond $z > 2.5$ this indicates that the early universe was extremely dense and energetic. As redshift decreases, i.e., the universe evolves, both $p(z)$ and $\varepsilon(z)$ decrease, suggesting a cooling and expanding universe. The energy density $\varepsilon(z)$ is consistently greater than pressure $p(z)$, showing it dominates the dynamics. At present (low z), both values are very low, pointing toward a diluted universe. This behavior aligns with a universe that began in a hot, dense state and is now expanding and cooling.

4.1 Deceleration Parameter

The acceleration of the universe can be quantified through a dimensionless cosmological function known as the 'deceleration parameter'. Solving eq. (20) by using eq. (27) in terms of redshift is given by

$$q(z) = -1 - \frac{rk_2^{\alpha}}{\gamma(1+z)^{\alpha}} - \frac{k_1 r}{\gamma} + \alpha \qquad (34)$$

The deceleration gives a measure of the rate at which the expansion of the universe is taking place. The positive sign of q corresponds to the standard decelerating model, whereas the negative sign of q indicates inflection and $q = 0$ the expansion of the universe at a constant rate.

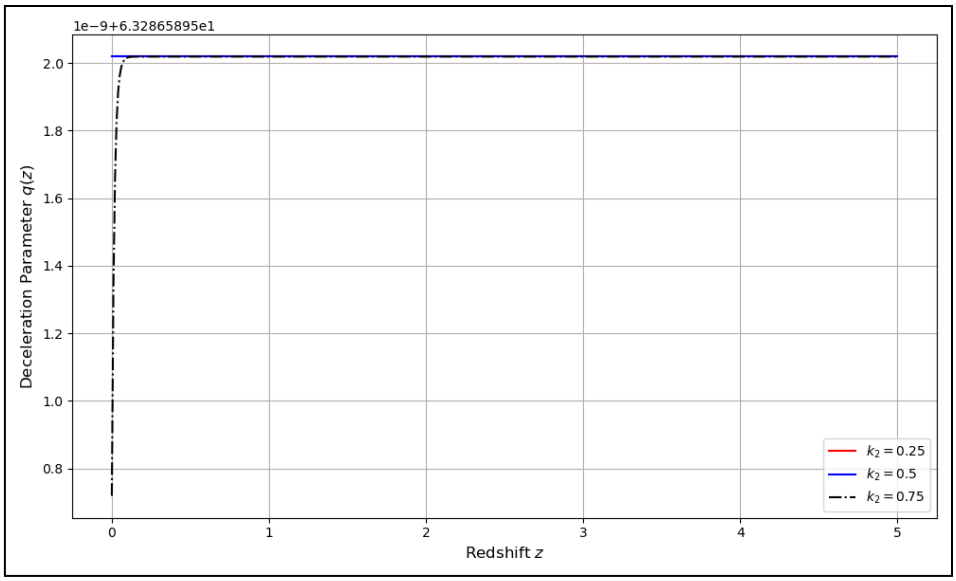

Fig. 5: Deceleration Parameter Vs. redshift for $k_1 = -1, \gamma = 0.743, \alpha = 64.152, r = 0.1$

From fig. 5, we can observed that the deceleration parameter $q(z)$ are in positive and almost constant for all values of k_2. At low redshift $(z \approx 0)$, a steep reduction in $k_2 = 0.75$ indicates rapid early evolution. However, for all cases, $q(z) > 0$, meaning the universe does not enter an accelerating phase. The curves immediately stabilize after a modest z, indicating that deceleration remains almost constant at greater redshifts. This pattern implies that the universe is dominated by matter or similar stuff, with no influence from dark energy or cosmic acceleration.

4.2 Jerk Parameter

The jerk parameter (j) is defined as

$$j = \frac{1}{aH^3}\frac{d^3a}{dt} \tag{35}$$

Where, a is dimensionless and third derivative of the scale factor with respect to redshift z The transition of the universe from decelerating to the accelerating phase, for various models of the cosmos, has a variation in the transition of the universe whenever the jerk parameter lies in the positive region and the deceleration parameter lies in the negative region. Visser [53] Rapetti *et al.,* [54] showed that for the flat $\wedge CDM$ model, the value of jerk becomes unity.

For solving eq. (35) we get

$$j(z) = -\frac{6\alpha^3 k_2^{3\alpha}}{\gamma^3(1+z)^{3\alpha+3}} \tag{36}$$

4.3 Snap Parameter $(\bar{S})$

The snap parameter, denoted as $(\bar{s})$, captures the rate of change of jerk with time and is expressed as

$$\bar{s} = \frac{\dddot{a}}{aH^4} \tag{37}$$

While the snap parameter is less commonly discussed compared to deceleration and jerk, it offers valuable insights into the finer details of cosmic dynamics, especially in scenarios where precise measurements are crucial for testing theoretical predictions. These parameters collectively provide a comprehensive framework for characterizing the evolution of the universe and investigating the underlying physics governing its behaviour.

Solving eq. (37) we get,

$$\bar{s} = \frac{24\alpha^4 k_2^{4\alpha}}{\gamma^4(1+z)^{4\alpha+4}} \tag{38}$$

4.4 Statefinder Diagnostic

Statefinder diagnostic parameters are dimensionless quantities used in cosmology to characterize the evolution of the universe and provide insights into the nature of dark energy in the universe. The dark energy models can be detected with the help of the state finder diagnostic pair $\{r, s\}$ which gives us an idea about the geometrical nature of the model. Sahni *et al.,*[55], Alam *et al.,*[56]. This geometrical pair is represented as (r, s), and are formulated as

$$r = \frac{\dddot{a}}{aH^3} \;\&\; s = \frac{r-1}{3\left(q - \frac{1}{2}\right)} \tag{39}$$

Where r is the same as that of the jerk parameter and s is the combination of r and s the deceleration parameter q. These statefinders defines $\wedge CDM$ and standard cold dark matter (CDM), respectively. However, $s > 0$ and $r < 1$ constitute the dark energy regions such as phantom and quintessence, $s < 0$ and $r > 1$ give the Chaplying gas model. We have obtained expressions for the statefinder diagnostic pair (r, s) for the models Bianchi type- II, which is given by

$$r = -\frac{6\alpha^3 k_2^{3\alpha}}{\gamma^3(1+z)^{3(\alpha+1)}} \;\&\; s = \left[\frac{4\alpha^3 k_2^{3\alpha}\gamma(1+z)^{\alpha}}{2rk_2^{\alpha} + [2k_1 r - 2\alpha\gamma + 3\gamma](1+z)^{\alpha}}\right] \tag{40}$$

4.5 Om (z) diagnostics

The starting point for Om (z) diagnostics is the Hubble parameter, it is defined as

$$Om(z) = \frac{\left(\frac{H_z}{H_0}\right)^2 - 1}{(1+z)^3 - 1} \tag{41}$$

Thus, $Om(z)$ involves only the first derivative of the scale factor through the Hubble parameter and is easier to reconstruct from observational data gives

$$Om(z) = \frac{\gamma^2(1+z)^{2\alpha} - H_0^2\alpha^2 k_2^{2\alpha}}{\alpha^2 k_2^{2\alpha} H_0^2\left((1+z)^3 - 1\right)} \tag{42}$$

4.6 Hubble Datasets

Measurement of dt yields the Hubble parameter, which is independent of the model, as the Hubble parameter is also related to the differential redshift, as $H(z) = -\frac{1}{(1+z)}\frac{dz}{dt}$ where dz is acquired from the spectroscopic surveys. Actually, there are two common approaches to determining the Hubble

parameter values $H(z)$ at a given redshift: a differential age (DA) and the line-of-sight baryonic acoustic oscillation (BAO) datasets. The 57 newest $H(z)$ data points in the redshift range of $0.070 \le z \le 2.36$ provide observational constraints on parameters $H_0 = \in (\lambda + 1)$. The DA technique was used to collect 31 points, the BAO technique was used to collect 26 points. A list of 57 $H(z)$ values in the redshift range $0.070 \le z \le 2.36$ has been proposed in [57-58] (see Table 1). We found the best-fit curve of $H(z)$ with 57 data values shown in Table 1, using the $R^2 - test$:

$$R^2 = 1 - \frac{\sum_{i=1}^{57}\left[(H_i)_{obs} - (H_i)_{th}\right]^2}{\sum_{i=1}^{57}\left[(H_i)_{obs} - (H_i)_{mean}\right]^2} \qquad (43)$$

The $R^2 - test$ examines how much of the universe in the dependent variable can be explained by the independent variable. Regarding the values of model parameters H_0, δ and λ in relation to the observatory Hubble dataset (HOD), a $R^2 = 1$ denotes an exact fit. To determine the optimal values of H_0, δ and λ, we limit the parametric spaces $-1 < z$ and $\in \neq 0$. For $H_0 = 67.8 kms^{-1}Mpc^{-1}$, $\Omega_m = 0.3$ and $\Omega_\Lambda = 0.7$, the error bars show the mean point and how far it is from the mean across 57 points of the Hubble dataset $H(z) = H_0\sqrt{\Omega_m(1+z)^3 + \Omega_\Lambda}$. Here, Ω_m and Ω_Λ are the density parameters of dark matter dark energy, respectively. For appximate values of $H_0 = 64.49^{+0.33}_{-0.32}, \gamma = 64.152^{+1.118}_{-1.118}, \alpha = 0.743^{+0.024}_{-0.024}$, we obtain the best-fit plot with a maximum of $R^2 = 0.9321$ and a root mean square error (RMSE) of 11.071.

z	$H(z)$	σ_H	Ref.	z	$H(z)$	σ_H	Ref.
0.070	69	19.6	[59]	1.750	202	40	[60]
0.90	69	12	[60]	1.965	186.5	50.4	[65]
0.120	68.6	26.2	[59]	0.24	79.69	2.99	[66]
0.170	83	8	[60]	0.30	81.7	6.22	[67]
0.1791	75	4	[61]	0.31	78.18	4.74	[68]
0.1993	75	5	[61]	0.34	83.8	3.66	[66]
0.200	72.9	29.6	[62]	0.35	82.7	9.1	[64]
0.270	77	14	[60]	0.36	79.94	3.38	[68]
0.280	88.8	36.6	[62]	0.38	81.5	1.9	[69]
0.3519	83	14	[61]	0.40	82.04	2.03	[68]
0.3802	83	13.5	[63]	0.43	86.45	3.97	[66]
0400	95	17	[60]	0.44	82.6	7.8	[70]
0.4004	77	10.2	[63]	0.44	84.84	1.83	[68]
0.4247	87.1	11.2	[63]	0.48	87.79	2.03	[68]
0.4497	92.8	12.9	[63]	0.51	90.4	1.9	[69]
0.470	89	34	[64]	0.52	94.35	2.64	[68]
0.4783	80.9	9	[63]	0.56	93.34	2.3	[68]
0.480	97	62	[59]	0.57	87.6	7.8	[71]
0.593	104	13	[61]	0.57	96.8	3.4	[72]
0.6797	92	8	[61]	0.59	98.48	3.18	[68]
0.7812	105	12	[61]	0.60	87.9	6.1	[70]
0.8754	125	17	[61]	0.61	97.3	2.1	[69]
0.880	90	40	[59]	0.64	98.82	2.98	[68]
0.900	117	23	[60]	0.73	97.3	7.0	[70]
1.037	154	20	[61]	2.30	224	8.6	[73]
1.300	168	17	[60]	2.33	224	8	[74]
1.363	160	33.6	[65]	2.34	222	8.5	[73]
1.430	177	18	[60]	2.26	226	9.3	[75]
1.530	140	14	[60]				

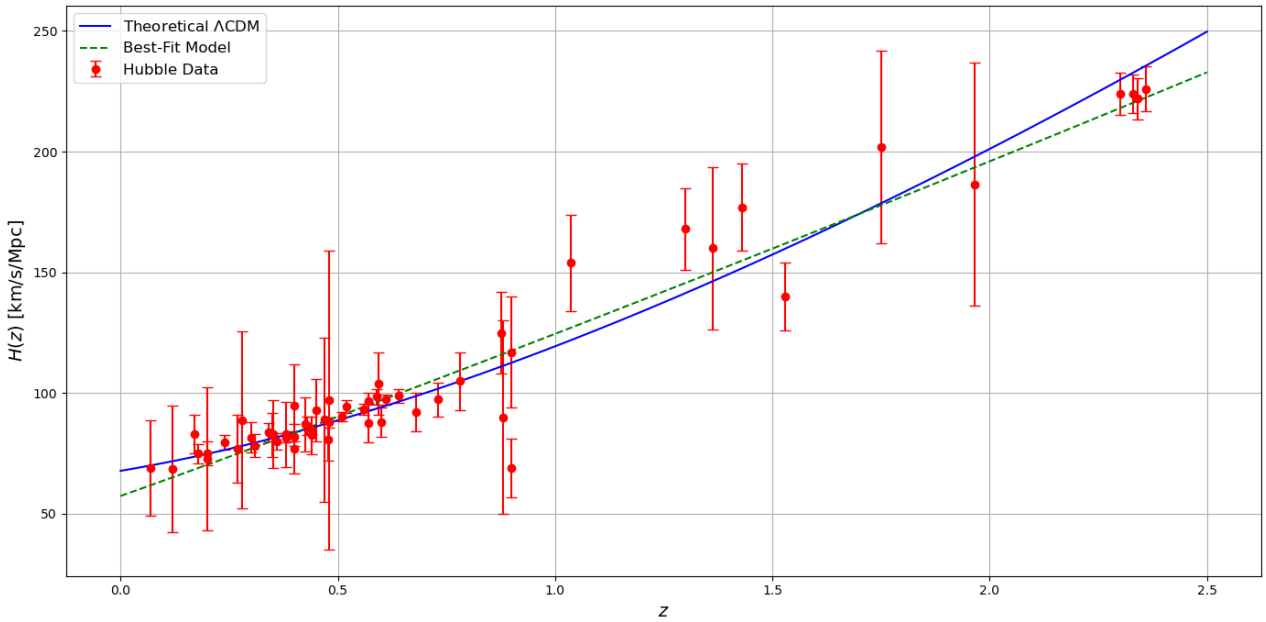

Fig 6. Hubble parameter (H) Vs. redshift (z) along with Hubble data set given in Table 1.

Fig. (6), it is observed that the Hubble parameter $H(z)$ increasing with redshift z , indicating that the universe expanded faster in the past. At low redshift, the expansion slows down, showing late-time acceleration. The observational Hubble data (red points) generally agree with both the ΛCDM model (blue line) and the best-fit model (green dashed line). This confirms the accelerated expansion of the universe due to dark energy. The ΛCDM model fits well across the full redshift range. The large error bars at higher z indicate observational uncertainties. Overall, the universe transitions from decelerated to accelerated expansion over time.

CONCLUSION

In this paper, we investigated the Bianchi type II space time cosmological model in scalar tensor theory of gravitation proposed by Brans-Dicke theory with a microscopic body. To solve the Brans-Dicke field equation by using the relation between metric potential and radiation of universe. Also, using a generalized law for the deceleration parameter, this allows for a time-varying deceleration scenario. And then we obtain exact solutions for the metric functions and scalar field.

The cosmological parameters, including the Hubble parameter, expansion scalar, shear scalar, energy density, pressure, and scalar field, are determined as redshift functions. The Hubble parameter, expansion scalar and shear scalar all increase with redshift, indicating the rapid early expansion of the universe. The scalar field grows increasing negative as redshift increases, indicating more dynamic gravitational influences in the early universe. Pressure and energy density both grow rapidly at higher redshifts and decrease over time, lending credence to the idea of a developing and cooling universe. From fig., (5) it is observed that deceleration parameter (q) indicates whether the universe is accelerating or decelerating in its expansion. At $z = 0$, the deceleration parameter (q) is negative, which suggests that the universe is currently undergoing accelerated expansion.

The analysis of jerk and snap parameters shows consistency with recent observational data and helps track the transition from deceleration to acceleration. The statefinder diagnostics utilizing the pair $\{r, s\}$ indicate divergence from the ΛCDM model, implying that the model may capture effects connected with non-standard dark energy forms, such as quintessence. we have also obtained the Om diagnostics, which were a useful test for comparing the model to the conventional ΛCDM model. Also, it is observed that best-fitted curve closely matched the data points when we compared the graph of the Hubble parameter with the Hubble dataset, we use a collection of 57 observational Hubble parameter data points that were gathered using BAO and differential age approaches in order to evaluate the theoretical model. The observational feasibility of the model is confirmed by the best-fit curve, which displays excellent agreement with a coefficient of determination $R^2 = 0.9321$ and a root mean square error of roughly 11.07.

REFERENCES

1. Brans, C., & Dicke, R. H. (1961). Mach's principle and a relativistic theory of gravitation. Physical review, 124(3), 925.
2. Sharma, M., Vicente, G. S., Graef, L. L., Ramos, R. O., & Wang, A. (2025).Quantum geometric

formulation of Brans-Dicke theory for Bianchi I spacetime. Physical Review D, 111(4), 043501.13
3. Ahmadi-Azar, E., Atazadeh, K., & Eghbali, A. (2024). Linear independence of field equations in the Brans-Dicke theory. arXiv preprint arXiv:2410.13316.
4. MISHRA, R. K., & Sharma, R. (2024). Investigating the Bianchi IX universe within Brans Dicke theory & a novel deceleration parameter.
5. Santhi, M. V., & SantoshRupa, K. (2024). Study on Anisotropic Dark Energy Cosmological Models in Generalized Brans-Dicke Theory. East European Journal of Physics, (3), 103-115.
6. Satyanarayana, P. E., & Sireesha, K. V. S. (2024). Bianchi Type-III Viscous Holographic Ricci Dark energy Cosmological model in Brans-Dicke theory of Gravitation. East European Journal of Physics, (1), 127-135.
7. Gaidhane, P. W., Pund, A. M., & Lambat, P. M. (2024). Anisotropy Bianchi Type-III Cosmological Model in Brans-Dicke Theory of Gravitation. Indian Journal of Science and Technology, 17(18), 1868-1879.
8. Bamba, K., Bhatti, M. Z., Yousaf, Z., & Shoukat, Z. (2023). Gravitational decou-pling of anisotropic stars in the Brans–Dicke theory. The European Physical Journal C, 83(11), 1033.
9. Nimkar, A. S., Hadole, S. R., & Wath, J. S. (2023). Cosmological model in Brans–Dicke theory of gravitation. Indian Journal of Physics, 97(5), 1633-1640
10. Çağlar, H. (2023). An Investigation into LRS Bianchi I Universe in Brans-Dicke Theory. Journal of New Theory (44), 87-96. https://doi.org/10.53570/jnt.1352470
11. Vijaya Santhi, M., Chinnappalanaidu, T., & Srivani Madhu, S. (2023). Viscous Ricci Dark Energy Cosmological Models in Brans-Dicke Theory. Astrophysics, 66(4), 559-589.
12. Santhi, M. V., Chinnappalanaidu, T., Madhu, S. S., & Gusu, D. M. (2022).Some Bianchi type viscous holographic dark energy cosmological models in the Brans–Dicke theory. Advances in Astronomy, 2022(1), 5364541.
13. Kapse, D. V., & Katore, S. D. (2022). Evolution of Viscous Dark Energy Models in Brans-Dicke Theory of Gravitation. Bulgarian Journal of Physics, 49(4).
14. Bhardwaj, V. K., Dixit, A., & Pradhan, A. (2023). Bianchi type-V transition- ing model in Brans–Dicke theory with observational constraints. International Journal of Geometric Methods in Modern Physics, 20(02), 2350022.
15. Trivedi, D., & Bhabor, A. K. (2021). Higher dimensional Bianchi type-III string cosmological models with dark energy in Brans-Dicke scalar-tensor theory of gravitation. New Astronomy, 89, 101658.14
16. Singh, C. P., & Sol`a Peracaula, J. (2021). Friedmann cosmology with decaying vacuum density in Brans–Dicke theory. The European Physical Journal C, 81(10), 960.
17. Singh, S. S., & Soibam, Y. (2021). Anisotropic models with generalized hybrid expansion in Brans–Dicke theory of gravity. International Journal of Geometric Methods in Modern Physics, 18(09), 2150141.
18. Singh, G. P., Lalke, A. R., & Hulke, N. (2020). Some Bianchi I dark energy models in Brans–Dicke theory. Pramana, 94(1), 147.
19. Saha, B. (2013). Some remarks on Bianchi type-II, VIII, and IX models. Gravitation and Cosmology, 19, 65-69.
20. Shaikh, A. Y. (2020). Viscous Dark Energy Cosmological Models in Brans-Dicke Theory of Gravitation. Bulgarian Journal of Physics, 47.
21. Rani, N. S., Sireesha, K. V. S., & Rao, V. U. M. (2019, October). Bianchi type-III, V and VI0 generalized ghost dark energy models with polytropic gas in Brans-Dicke theory of gravitation. In Journal of Physics: Conference Series (Vol. 1344, No. 1, p. 012045). IOP Publishing.
22. Pawar, D. D., Shahare, S. P., & Dagwal, V. J. (2018). Tilted Kantowski–Sachs cosmological model in Brans–Dicke theory of gravitation. Modern Physics Letters A, 33(04), 1850011.
23. Tirandari, M., & Saaidi, K. (2017). Anisotropic inflation in Brans–Dicke gravity.Nuclear Physics B, 925, 403-414.
24. Rao, V. U. M., Suryanarayana, G., & Aditya, Y. (2016). Kantowski-Sachs two fluid radiating cosmological model in Brans-Dicke theory of gravitation. Advances in Astrophysics, 1, 62-71.
25. Chirde, V. R., & Kadam, V. P. (2016). Bianchi Type V Cosmological Model with Wet Dark Fluid in Brans-Dicke Theory of Gravitation. International Journal for Innovative Research in Sciences & Technology, 3(5), 63-68.
26. Chirde, V. R., & Kadam, V. P. (2016). Bianchi Type III Cosmological models with strange Quark matter attached to string cloud in Brans-Dicke Theory of gravitation and general theory of relativity. Caribbean Journal of Sciences and Technology, 4(1), 920-930.
27. Pawar, D. D., & Dagwal, V. J. (2015). Tilted Kasner-type Cosmological models in Brans-Dicke theory of gravity. Prespacetime Journal, 6(11).
28. Pawar, D. D., & Solanke, Y. S. (2014). Exact kantowski-sachs anisotropic dark energy cosmological models in brans dicke theory of gravitation. International 15 Journal of Theoretical Physics, 53, 3052-3065.
29. Reddy, D. R. K., Bharati, D., & Vijaya Lakshmi, G. V. (2014). Kantowski–Sachs bulk viscous string cosmological model in Brans–Dicke theory of gravitation. Astrophysics and Space Science, 351, 307-311.
30. Reddy, D. R. K., & Vijaya Lakshmi, G. V. (2014). Five dimensional radiating model in Brans-Dicke

theory of gravitation. Astrophysics and Space Science, 354,633-636.
31. Wankhade, K. S., & Sancheti, M. M. (2014). Bianchi Type II, VIII & IX Cosmo-logical Model with Magnetized Anisotropic Dark Energy in Brans-Dicke Theory of Gravitation. International Journal of Theoretical Physics, 53(8), 2836-2845.
32. Vidyasagar, T., Naidu, R. L., Bhuvana Vijaya, R., & Reddy, D. R. K. (2014). Bianchi type-VI 0 bulk viscous string cosmological model in Brans-Dicke scalar- tensor theory of gravitation. The European Physical Journal Plus, 129, 1-7.
33. Vidyasagar, T., Purnachandra Rao, C., Bhuvana Vijaya, R., & Reddy, D. R. K. (2014). Bianchi type-III bulk viscous cosmic string model in a scalar-tensor theory of gravitation. Astrophysics and Space Science, 349, 467-471.
34. Ghate, H. R., & Sontakke, A. S. (2013). Bianchi Type-IX Dark Energy Model in Brans-Dicke Theory of Gravitation. Prespacetime Journal, 4(4).
35. Adhav, K. S., Ugale, M. R., Kale, C. B., & Bhende, M. P. (2009). Plane Sym- metric Vacuum Bianchi Type-III Cosmological Model in Brans-Dicke Theory. International Journal of Theoretical Physics, 48, 178-182.
36. Adhav, K. S., Nimkar, A. S., Ugale, M. R., & Dawande, M. V. (2008). BianchiType-III cosmological model with negative constant deceleration parameter in Brans Dicke theory of gravitation. International Journal of Theoretical Physics, 47, 634-639.
37. Tinker, S. (2021). Inflationary Bianchi type-II space-time with exponentialpoten-tial. GANITA, 71(1), 235-242.
38. Chirde, V. R., & Shekh, S. H. (2019). Dynamics of magnetized anisotropic dark energy in f (R, T) gravity with both deceleration and acceleration. Bulg. J. Phys, 46, 94-106.
39. Bhoyar, S. R., Chirde, V. R., & Shekh, S. H. (2018). Maximal Coupling of Bianchi Type-II, VIII and IX Space-Time with HDE and DM in Gravity. International journal of scientific Research in physics and Applied Sciences 6(6) 139-145 (2018)
40. Sharma, N. K., & Singh, J. K. (2014). Bianchi type-II String Cosmological Model with Magnetic Field in Scale-Covariant Theory of Gravitation. International Journal of Theoretical Physics, 53, 4132-4140.
41. Singh, J. K., & Sharma, N. K. (2014). Bianchi type-II dark energy model in scale covariant theory of gravitation. International Journal of Theoretical Physics, 53,461-468.
42. Singh, J. K., & Sharma, N. K. (2014). Anisotropic dark energy Bianchi Type-II cosmological models in Lyra geometry. International Journal of Theoretical Physics, 53, 1375-1386.
43. Pradhan, A., Amirhashchi, H., & Jaiswal, R. (2011). A new class of LRS Bianchi type-II dark energy models with variable EoS parameter. Astrophysics and Space Science, 334, 249-260.
44. Agarwal, S., Pandey, R. K., & Pradhan, A. (2011). LRS Bianchi type II per-fect fluid cosmological models in normal gauge for Lyra's manifold. International Journal of Theoretical Physics, 50, 296-307.
45. Singh, J. K., & Sharma, N. K. (2010). Some Bianchi type-II cosmological models in Brans–Dicke theory. Astrophysics and Space Science, 327, 293-298.
46. Banerjee, A., Duttachoudhury, S. B., & Sanyal, A. K. (1986). Bianchi type-II cosmological model with viscous fluid. General relativity and gravitation, 18,461-477.
47. Wath, J. S., and Nimkar, A. S.(2024). Stability of Microscopic Body cosmological Model In Ruban's Background Jnanabha 54(1), 1-9.
48. Nimkar, A. S., & Hadole, S. (2023). Stability of Cosmological Model in Self-Creation Theory of Gravitation. Journal of Scientific Research, 15(1), 55-62.
49. Hadole, S. R.,Nimkar, A. S.(2022). Microscopic Body Cosmological Model Y M E R 21(5), 0044-0477.
50. Laundau, L. D., & Lifshitz, E. (1975). The classical theory of fields. 4th ed.(Butterworth-Heinemann.
51. Akarsu, ¨O., & Dereli, T. (2012). Cosmological models with linearly varying deceleration parameter. International Journal of Theoretical Physics, 51, 612-621.
52. Berman, M. S. (1983). A special law of variation for Hubble's parameter. Nuovo Cimento B Serie, 74, 182-186.
53. Visser, M. (2005). Cosmography: Cosmology without the Einstein equations.General Relativity and Gravitation, 37, 1541-1548.
54. Rapetti, D., Allen, S. W., Amin, M. A., & Blandford, R. D. (2007). A kinematical approach to dark energy studies. Monthly Notices of the Royal Astronomical Society, 375(4), 1510-1520.
55. Sahni, V., Saini, T. D., Starobinsky, A. A., & Alam, U. (2003). Statefinder—a new geometrical diagnostic of dark energy. Journal of Experimental and Theoretical Physics Letters, 77, 201-206.
56. Alam, U., Sahni, V., Deep Saini, T., & Starobinsky, A. A. (2003). Exploring the expanding universe and dark energy using the Statefinder diagnostic. Monthly Notices of the Royal Astronomical Society, 344(4), 1057-1074.
57. Dhore, A. O., & Ugale, M. R. (2025). Dark energy dynamics in teleparallel gravity with hyperbolic scale factor. Astrophysics and Space Science, 370(5), 41.
58. Arora, S., Pacif, S. K. J., Bhattacharjee, S., & Sahoo, P. K. (2020). f (Q, T) gravity models with observational constraints. Physics of the Dark Universe, 30,100664.
59. Stern, D., Jimenez, R., Verde, L., Kamionkowski, M., & Stanford, S. A. (2010). Cosmic chronometers: constraining the equation of state of dark energy. I: H (z) measurements. Journal of Cosmology and Astroparticle Physics, 2010(02), 008.

60. Simon, J., Verde, L., & Jimenez, R. (2005). Constraints on the redshift depen- dence of the dark energy potential. Physical Review D—Particles, Fields, Gravitation, and Cosmology, 71(12), 123001.
61. Moresco, M., Cimatti, A., Jimenez, R., Pozzetti, L., Zamorani, G., Bolzonella, M., & Welikala, N. (2012). Improved constraints on the expansion rate of the Universe up to z 1.1 from the spectroscopic evolution of cosmic chronometers. Journal of Cosmology and Astroparticle Physics, 2012(08), 006.
62. Zhang, C., Zhang, H., Yuan, S., Liu, S., Zhang, T. J., & Sun, Y. C. (2014). Four new observational H (z) data from luminous red galaxies in the Sloan Digital Sky Survey data release seven. Research in Astronomy and Astrophysics, 14(10), 1221.
63. Moresco, M., Pozzetti, L., Cimatti, A., Jimenez, R., Maraston, C., Verde, L.,& Wilkinson, D. (2016). A 6% measurement of the Hubble parameter at z0.45 direct evidence of the epoch of cosmic re-acceleration. Journal of Cosmology and Astroparticle Physics, 2016(05), 014.
64. Ratsimbazafy, A. L., Loubser, S. I., Crawford, S. M., Cress, C. M., Bassett, B. A., Nichol, R. C., & V¨ais¨anen, P. (2017). Age-dating luminous red galax- ies observed with the Southern African Large Telescope. Monthly Notices of the Royal Astronomical Society, 467(3), 3239-3254.
65. Moresco, M. (2015). Raising the bar: new constraints on the Hubble parameter with cosmic chronometers at z2. Monthly Notices of the Royal Astronomical Society: Letters, 450(1), L16-L20.
66. Gaztanaga, E., Cabre, A., & Hui, L. (2009). Clustering of luminous red galaxies–IV. Baryon acoustic peak in the line-of-sight direction and a direct mea- surement of H (z). Monthly Notices of the Royal Astronomical Society, 399(3), 1663-1680.
67. Oka, A., Saito, S., Nishimichi, T., Taruya, A., & Yamamoto, K. (2014). Simul-taneous constraints on the growth of structure and cosmic expansion from the multipole power spectra of the SDSS DR7 LRG sample. Monthly Notices of the Royal Astronomical Society, 439(3), 2515-2530.
68. Wang, Y., Zhao, G. B., Chuang, C. H., Ross, A. J., Percival, W. J., Gil-Mar´ın, H.,& Zhu, F. (2017). The clustering of galaxies in the completed SDSS-III Baryon Oscillation Spectroscopic Survey: tomographic BAO analysis of DR12 combined sample in configuration space. Monthly Notices of the Royal Astronomical Society, 469(3), 3762-3774.
69. Alam, S., Ata, M., Bailey, S., Beutler, F., Bizyaev, D., Blazek, J. A.,& Zhao, G. B. (2017). The clustering of galaxies in the completed SDSS-III Baryon Oscillation Spectroscopic Survey: cosmological analysis of the DR12 galaxy sample. Monthly Notices of the Royal Astronomical Society, 470(3), 2617-2652.
70. Blake, C., Brough, S., Colless, M., Contreras, C., Couch, W., Croom, S.,& Yee, H. K. (2012). The WiggleZ Dark Energy Survey: Joint measurements of the expansion and growth history at z¡ 1. Monthly Notices of the Royal Astronomical Society, 425(1), 405-414.
71. Chuang, C. H., Prada, F., Cuesta, A. J., Eisenstein, D. J., Kazin, E., Pad- manabhan, N.,& Thomas, D. (2013). The clustering of galaxies in the SDSS-III Baryon Oscillation Spectroscopic Survey: single-probe measurements and the strong power of f (z)σ8(z) on constraining dark energy. Monthly Notices of the Royal Astronomical Society, 433(4), 3559-3571.
72. Anderson, L., Aubourg, E., Bailey, S., Beutler, F., Bhardwaj, V., Blanton, M.,& Zhao, G. B. (2014). The clustering of galaxies in the SDSS-III Baryon Oscillation Spectroscopic Survey: baryon acoustic oscillations in the Data Releases 10 and 11 Galaxy samples. Monthly Notices of the Royal Astronomical Society, 441(1), 24-62.
73. Delubac, T., Rich, J., Bailey, S., Font-Ribera, A., Kirkby, D., Le Goff, J. M.,& York, D. G. (2013). Baryon acoustic oscillations in the Lyα forest of BOSS quasars. Astronomy & Astrophysics, 552, A96.
74. Bautista, J. E., Guy, J., Rich, J., Blomqvist, M., Des Bourboux, H. D. M., Pieri, M. M.,& Y`eche, C. (2017). Measurement of baryon acoustic oscillation correla- tions at z= 2.3 with SDSS DR12 Lyα-Forests. Astronomy & Astrophysics, 603, A12.
75. Font-Ribera, A., Kirkby, D., Miralda-Escud´e, J., Ross, N. P., Slosar, A., Rich, J.,&York, D. G. (2014). Quasar-Lyman α forest cross-correlation from BOSS DR11: Baryon Acoustic Oscillations. Journal of Cosmology and Astroparticle Physics, 2014(05), 027.